AUT Journal of Electrical Engineering

AUT J. Elec. Eng., 54(1) (2022) 121-136
DOI: 10.22060/eej.2021.20393.5429

Simplified Model Predictive for Controlling Circulating and Output Currents of a Modular Multilevel Converter

A. Sheybanifar, S. M. Barakati*

Department of Electrical and Computer Engineering, University of Sistan and Baluchestan, Zahedan, Iran

ABSTRACT: Model Predictive Control (MPC) has attracted wide attention recently, especially in electrical power converters. MPC advantages include straightforward implementation, fast dynamic response, simple system design, and easy handling of multiple objectives. In conventional MPC, the optimal value of the cost function is obtained after calculating all switching states, which makes this method impossible to implement. In this paper, a Simplified Model Predictive Control (S-MPC) is presented to control the circulating and output currents in a Modular Multilevel Converter (MMC). Using a discrete mathematical model of MMC and the neighboring index values with respect to their previously applied values, the calculation burden can be reduced rapidly, and even the number of Sub-Modules (SMs) increases. The conventional MPC is expressed for comparison with the proposed method. In addition, a bilinear mathematical model of the MMC is derived and discretized to predict the states of the MMC for one step ahead. A sorting algorithm is used to retain the balancing capacitor voltage in each SM, while the cost function guarantees the regulation of the output current, and MMC circulating current. In the simulation section, the proposed method is implemented in a three-phase MMC with four SMs in each arm. The accuracy and performance of the proposed method are evaluated with simulation and experimental results.

Review History:

Received: Aug. 12, 2021
Revised: Dec. 13, 2021
Accepted: Dec. 14, 2021
Available Online: Jun. 01, 2022

Keywords:

Modular multilevel converter
Model predictive control
Computational load
Voltage balancing
Improving dynamic response.

1- Introduction

Power Electronic converters are used in a variety of applications; these include in various industries such as HVDC systems, renewable energy, machine drives, aerospace, and spacecraft power systems [1-5]. In general, power electronic converters are divided into two categories: conventional converters and Multilevel Converters (MLCs). Due to requiring large capacitive-inductive filters in the AC side to remove the output current ripple, conventional converters may not have the appropriate performance [6]. On the other hand, to improve power quality, it is needed to use complex switching algorithms, such as Space Vector Modulation (SVM), which complicate the control system [7]. MLCs are suitable substitutes for conventional converters, especially in high-power applications, without the need for the capacitive-inductive filter [8]. Due to using a large number of switches in these converters, the ripples of the current and voltage are very low. Moreover, by increasing the number of switches in MLCs, there is no need to increase the switching frequency to reduce the voltage ripple, hence the system performance is improved as well as the efficiency is increased. These structures have different disadvantages, for instance in Cascade H-bridge structure (CHB), a large number of DC voltage sources is needed. Additionally, the diode clamp and Fly Capacitor (FC) structures suffer from practical implementation problems and the high cost of equipment [9].

Therefore, another type of Multilevel Converters, called Modular Multilevel Converters (MMCs), have been entered into the electric industry. These converters exhibit several attractive features for the medium and high-power applications, such as straightforward scalability, voltage and current waveforms with very low harmonic content and high availability as well as fault tolerance [6]. There is a voltage unbalance in the capacitors in MMC, which is necessary to use linear or non-linear control methods to control them [6]. To balance the capacitor voltage, a mathematical method is used in [10]. In this method, the individual capacitor voltage regulation is implemented based on Phase-Shifted-Carrier Pulse-Width Modulation (PSC-PWM). In addition, based on the consensus theory, the influence of different communication structures on the MMC voltage regulation performance is discussed.

In [11]. , the finite control set MPC (FCS-MPC) is used to control the parameter of MMC. In FCS-MPC, due to the consideration of all switching states, with increasing the number of SMs, the computational burden is increased. For computational volume reduction, the indirect finite control set MPC (IFCS-MPC) is applied in [12]. In IFCS-MPC, the sorting algorithm balances capacitors voltages; hence, the number of switching states has been reduced to $(N+1)^2$, where N is the number of SMs. In [13], optimal predictive control is present-

*Corresponding author's email: vmashayekhi@shahroodut.ac.ir

Table 1. The SMs Mode of MMC

SM mode	S_1	S_2	V_{SM}
On-mode	ON	OFF	$V_{cmi,j}$
Off-mode	OFF	ON	0

ed to reduce the volume of calculations. In this method, by cost function optimization in each step and combining with the sorting algorithm, the output current and the voltages of the capacitors are controlled. In this method, the switching states are reduced, but are dependent on the number of SMs. By combining the predictive control method with Phase-Shift Pulse Width Modulation (PS-PWM) in [14], the number of switching states is significantly reduced, and the output current ripples are limited. By minimizing the switching states and optimizing the duty cycle in each step, the circulating current and output current errors are minimized, and the dynamic response is increased despite the constant frequency. However, by increasing the number of SMs, the switching states are increased. In [15], an improved prediction control algorithm is presented for the application on MMC. In this method, first a mathematical model of MMC is presented. Afterwards, the stability analysis of the current control loop is obtained, and the control boundary gain of the controller is determined. This algorithm can reduce the high computational volume of the predictive control method. In addition, to limit the prediction error, a repetitive controller is provided to control the capacitor's voltages of the SMs. By increasing the number of SMs, the computational volume is reduced, but the complexity of this method is increased.

From the mentioned methods, it can be concluded that by increasing the number of SMs, the complexity of the control system and the computational burden are increased, and the implementation of these methods had some challenges.

In this paper, a bilinear mathematical model of the MMC is developed, and the simplified model predictive control is applied to control the output current and circulating current. In fact, in the proposed method, due to the significant reduction in the number of switching modes compared to the mentioned methods, the computational burden of MPC is separated from the switching modes number. In other words, switching modes do not change with the number of SMs. This simplifies the control system and can be used in medium and high-power industrial converters.

In addition, using the proposed method reduces the disturbances of the output and the circulating currents. Therefore, the performance of the closed-loop control system increases. Additionally, to control the voltages of capacitors, the sorting algorithm is used.

The rest of the paper is organized as follows: Section 2 presents the topology, basic operation, and a bilinear mathematical model of MMC. In Section 3, the details of the proposed S-MPC, and the conventional MPC are explained. Section 4 and 5 show the simulation and experimental results of the proposed method on the MMC, respectively. Finally, in Section 6, conclusions are presented.

2- Mathematical Model of MMC

The topology of the three-phase MMC is shown in Fig. 1. This structure consists of three legs, where each leg has two arms: upper and lower arms are represented by the subscript "up" and "low", respectively. There are N SMs in each arm which represent the number of SMs. The structure of the SMs in the arm is considered half-bridge, due to efficiency and low cost [13]. The inductance (L_{arm}) in the arm is used to limit the di/dt of circulating current, and the resistance of the arm also indicates the losses of the arm. On the AC side, it is assumed that the converter is connected to the AC grid with voltage ($V_{t,j}$), impedance $L_{t,j}$, and $R_{t,j}$ where j represents each of the phases (a, b, c). It is assumed that the capacitor's voltages of the SMs are balanced.

The switching states of the SMs are generally on-state and off-state. In on-state mode, the output voltage of the SM is $V_{cmi,j}$ (m=1, 2... N, i = up, low), when S_1 is turned on, and S_2 is off. Additionally, in off-state, the output voltage of the SM is zero when S_1 is turned off, and S_2 is on. Table 1 shows the switching states of SMs.

The capacitor voltage dynamic equation for each SM of the MMC is expressed as follows:

$$\frac{dV_{cmi,j}}{dt} = i_{ci,j} \Big/ C_{SM} \tag{1}$$

where C_{SM} is the capacitance of the SM, and $i_{ci,j}$ is the capacitor current, which can be obtained from the switching state $S_{mi,j}$ and the arm current $i_{i,j}$ as follows:

$$i_{ci,j} = S_{mi,j}\, i_{i,j} \tag{2}$$

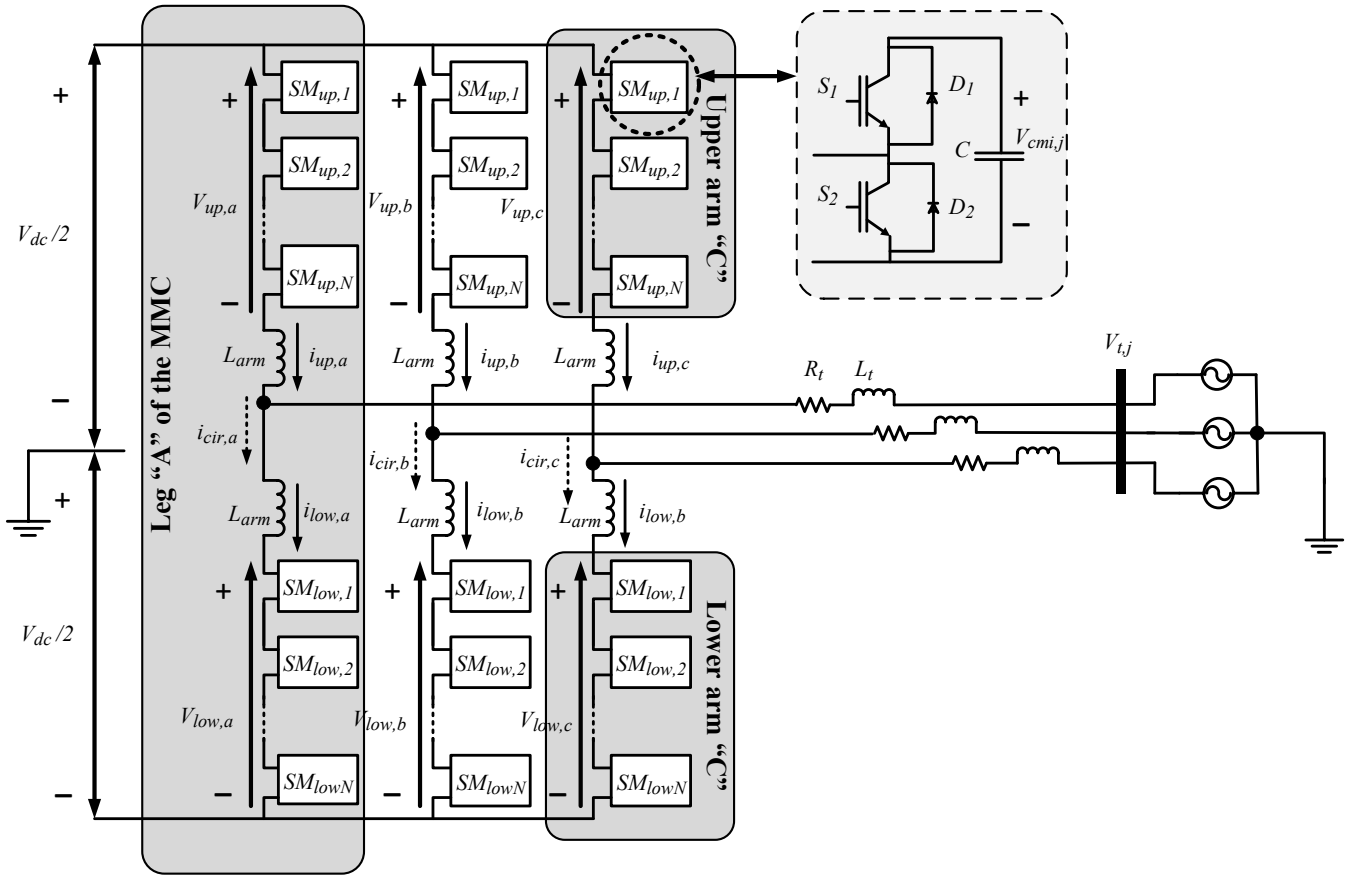

Fig. 1¬. The three-phase MMC structure with N SMs in each arm

The state-space equations describing the MMC can be expressed by [13]:

$$\frac{V_{dc}}{2}-V_{low,j}-R_{arm}i_{low,j}-L_{arm}\frac{di_{low,j}}{dt}+ R_{t,j}i_{t,j}+L_{t,j}\frac{di_{t,j}}{dt}+V_{t,j}=0 \tag{3}$$

$$-\frac{V_{dc}}{2}+V_{up,j}+R_{arm}i_{up,j}+L_{arm}\frac{di_{up,j}}{dt}+ R_{t,j}i_{t,j}+L_{t,j}\frac{di_{t,j}}{dt}+V_{t,j}=0 \tag{4}$$

In (3) and (4), $i_{t,j}$ is the current of the grid. Due to the symmetry between the upper and lower arm, the AC side current is divided equally between the upper and lower arm. The DC side current is divided into three parts due to the symmetry for the three phases. Hence, by using KCL, the upper and lower arm currents are as follow [13]:

$$i_{up,j}=\frac{I_{dc}}{3}+i_{cir,j}+\frac{i_{t,j}}{2} \tag{5a}$$

$$i_{low,j}=\frac{I_{dc}}{3}+i_{cir,j}-\frac{i_{t,j}}{2} \tag{5b}$$

As shown in (5a) and (5b), the upper and lower arm currents depend on the output current, the circulating current, and the DC side current. By combining (5a) and (5b), the circulating current and the AC side current are calculated as follows [13]:

$$i_{\mathrm{cir},j}=\frac{i_{up,j}+i_{low,j}}{2}-\frac{I_{dc}}{3} \tag{6}$$

$$i_{t,j}=i_{up,j}-i_{low,j} \tag{7}$$

Based on (6), the circulating current is contained of current DC component. Based on (3)(7), the state space equations are as follows:

$$\frac{di_{t,j}}{dt}=-\frac{R_{arm}+2R_{t,j}}{L_{arm}+2L_{t,j}}i_{t,j}+\frac{V_{low,j}-V_{up,j}-2V_{t,j}}{L_{arm}+2L_{t,j}} \tag{8}$$

$$\frac{di_{cir,j}}{dt}=-\frac{R_{arm}}{L_{arm}}i_{cir,j}+\frac{V_{dc}-V_{up,j}-V_{low,j}}{2L_{arm}} \tag{9}$$

where V_{up} and V_{low} are generated based on inserting and bypassing the special number of SMs. Assuming that the SMs capacitors voltages are well balanced at their reference values, the modulation indices determine the number of inserted SMs in each arm. Therefore, the arm voltages are expressed by:

$$V_{up,j}=\frac{n_{up,j}V^{\Sigma}_{cup,j}}{N} \tag{10}$$

$$V_{low,j}=\frac{n_{low,j}V^{\Sigma}_{clow,j}}{N} \tag{11}$$

where $n_{up,j}$ and $n_{low,j}$ are the modulation indices. By substituting (10) and (11) in (8) and (9), the state space equations are as follows:

$$\frac{di_{t,j}}{dt}=\frac{-\left(R_{arm}+2R_{t}\right)}{L_{arm}+2L_{t}}i_{t,j}+\frac{n_{low,j}v^{\Sigma}_{clow,j}-n_{up,j}v^{\Sigma}_{cup,j}}{N\left(L_{arm}+2L_{t}\right)}+\frac{2v_{t,j}}{L_{arm}+2L_{t}}. \tag{12}$$

$$\frac{di_{cir,j}}{dt}=-\frac{R_{arm}}{L_{arm}}i_{cir,j}-\frac{1}{2NL_{arm}}\left(n_{up,j}v^{\Sigma}_{cup,j}+n_{low,j}v^{\Sigma}_{clow,j}\right)+\frac{1}{2L_{arm}}V_{dc} \tag{13}$$

Therefore, the standard form of a continuous bilinear system is represented:

$$\dot{x}(t)=\underbrace{\begin{bmatrix}-\frac{R_{arm}+2R_{t}}{L_{arm}+2L_{t}} & 0 & 0 & 0\\ 0 & -\frac{R_{arm}}{L_{arm}} & 0 & 0\\ 0 & 0 & 0 & 0\\ 0 & 0 & 0 & 0\end{bmatrix}}_{A}x(t)+\underbrace{\begin{bmatrix}0 & 0 & \frac{1}{\left(L_{arm}+2L_{t,j}\right)N} & 0\\ 0 & 0 & -\frac{1}{2NL_{arm}} & 0\\ -\frac{1}{2C} & \frac{1}{C} & 0 & 0\\ 0 & 0 & 0 & 0\end{bmatrix}}_{B_1}u_1+\underbrace{\begin{bmatrix}0 & 0 & 0 & -\frac{1}{\left(L_{arm}+2L_{t,j}\right)N}\\ 0 & 0 & 0 & -\frac{1}{2NL_{arm}}\\ 0 & 0 & 0 & 0\\ \frac{1}{2C} & \frac{1}{C} & 0 & 0\end{bmatrix}}_{B_2}u_2+\underbrace{\begin{bmatrix}\frac{2v_{t,j}}{L_{arm}+2L_{t,j}}\\ \frac{V_{dc}}{2L_{arm}}\\ 0\\ 0\end{bmatrix}}_{d} \tag{14}$$

where $x=\left[i_{t,j}\ i_{cir,j}\ v^{\Sigma}_{up,j}\ v^{\Sigma}_{low,j}\right]^{T}$ is the state vector and $u=[u_1\ u_2]^{T}=[n_{up,j}\ n_{low,j}]^{T}$ is the control signal vector [16].

3- MPC Strategies for Modular Multilevel Converter

3- 1- Simplified Model Predictive Control

As mentioned, the model predictive can be used to control the MMC due to the ability to control multiple control targets by one cost function and its high dynamic response. In other words, the voltage of the capacitor, output current, and circulating current can be controlled by optimizing one cost function.

According to (12) and (13), based on the first-order expansion relation of Euler, the output and circulating currents equations for one step ahead are as follows:

$$i_{t,j}(k+1)=i_{t,j}(k)+\left(-\frac{R_{arm}+2R_{t,j}}{L_{arm}+2L_{t,j}}i_{t,j}(k)+\frac{n_{up,j}v^{\Sigma}_{cup,j}(k)-n_{low,j}v^{\Sigma}_{clow,j}(k)}{N\left(L_{arm}+2L_{t,j}\right)}+\frac{2v_{t,j}(k)}{L_{arm}+2L_{t,j}}\right)T_s \tag{15}$$

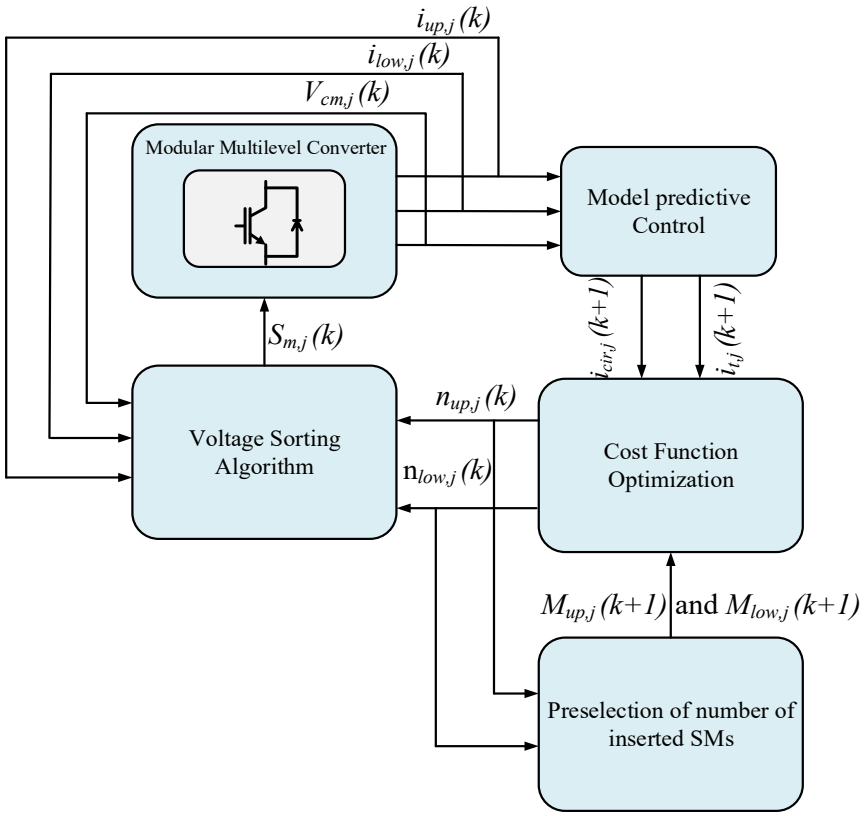

Fig. 2. Block diagram of the proposed method.

$$i_{cir,j}(k+1) = i_{cir,j}(k) + \begin{pmatrix} -\frac{R_{arm}}{L_{arm}} i_{cir,j}(k) - \\ \frac{1}{2NL_{arm}} \left(n_{up,j} v^{\Sigma}_{cup,j}(k) + \right) + \\ n_{low,j} v^{\Sigma}_{clow,j}(k) \\ \frac{1}{2L_{arm}} V_{dc} \end{pmatrix} T_s \quad (16)$$

Where $i_{t,j}(k)$ and $i_{cir,j}(k)$ are the measured values of the output current and the circulating current at the k instant. $i_{t,j}(k+1)$ and $i_{cir,j}(k+1)$ are the predicted values of output and circulating currents at k+1 instant. Also, T_s is the sampling time After evaluating all the correct switching states, the predicted values of output and circulating currents are placed in the cost function J, as follows:

$$J_j = \lambda_t \left| i_{t,j,\text{ref}}(k+1) - i_{t,j}(k+1) \right| + \lambda_{cir} \left| i_{cir,j,ref}(k+1) - i_{cir,j}(k+1) \right| \quad (17)$$

Where λ_{cir}, λ_t are the weighting coefficients of the circulating current and output current, respectively. Using the method in [17], the weighting coefficients for circulating current, and output current can be considered equal to (1) and (0.5), respectively. To operate the proposed method, for optimizing the cost function, the control modes $M_{x,j}$ (x = up, low) are selected and the optimal modulation indices ($n_{up,j}$ and $n_{low,j}$) are obtained for applying to the switches. In this method, the number of switching states is independent of the number of SMs and is equal to a maximum of three states (k-1, k, k + 1). Furthermore, the modulation indices at the end of each period are optimized. Fig. 2 and Fig. 3, show the block diagram and the flowchart of the proposed method, respectively.

Modulation indices ($n_{up,j}$, $n_{low,j}$) determine the output voltage levels. In this paper, voltage levels are generated by the cost function of the predictive control. In this method, along the generated modulation indices by the cost function, another part is applied to update these modulation indices, which is the preselection block. As shown in Fig. 2, the feedback is taken from the modulation indices at any instant in the preselection block, and the following step modulation indices are determined based on the previous step indices. The next state is effected by the previous state. When a new modulation index generates, a comparison is made between the new modulation index and the feedback index taken from the previous step. At any time, the generated modulation index has one of

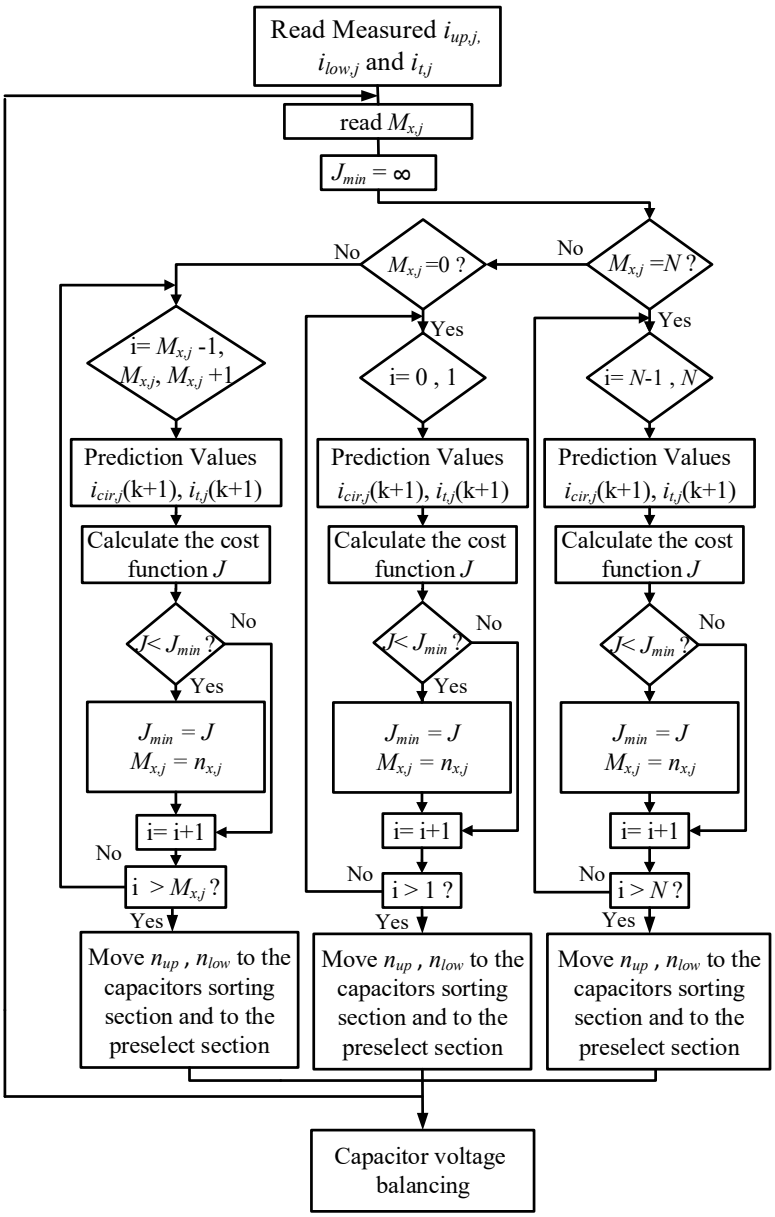

Fig. 3. Flowchart of the proposed method

the following three modes:

1. Suppose the new modulation index is at the N level (N is the number of SMs), and this value is the same as the previous modulation index. In that case, the prediction equations are calculated only for the N and N-1 states.

2. Suppose the new modulation index is at level 0, and this value is the same as the previous modulation index. In that case, the prediction equations are calculated only for two states, 0 and 1.

3. However, if the new modulation index has a value other than 0 and N, in this case, the new modulation index is not the same as the taken feedback modulation index, and the predictive equations are calculated for three different states. These three states depend on the taken feedback modulation index and are as follows:

$$M_{x,j-1}, M_{x,j}, M_{x,j+1}$$

The prediction equations are calculated for the above three values. The best state that optimizes the cost function is applied as the optimal modulation index to the voltages of the sorting section of the capacitor.

3- 2- Operation of Sorting Algorithm of Capacitor Voltages

In this paper, the voltage sorting algorithm in [12] is implemented to balance the capacitor's voltages of the MMC. According to Fig. 2, after generating the modulation indices from the cost function section, by a specify the number

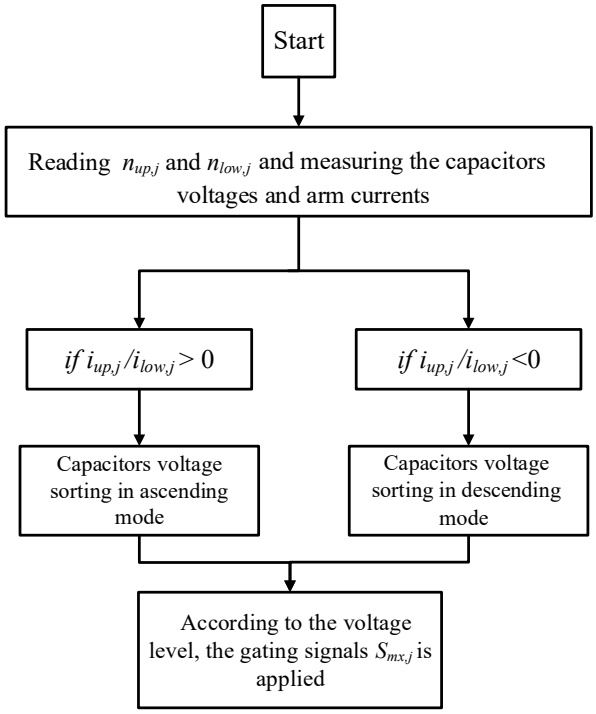

Fig. 4. Flowchart of the voltage sorting algorithm

of capacitors and based on the direction of current flowing through, the capacitor voltages are changed and should be updated for the next step. Hence, if the current arm is positive ($i_{up,j}/i_{low,j}>0$), the SMs with the lowest voltages in the respective arm and other SMs are bypassed, which is the ascending mode. On the other hand, if the current arm is opposing ($i_{up,j}/i_{low,j} < 0$), the SMs with the highest voltages in the respective arm and other SMs are bypassed, which is the descending mode. Hence, the switching signals ($S_{mx,j}$) are obtained to be applied in the sampling time k. Fig. 4 shows the operation of the voltage sorting algorithm.

3- 3- Conventional MPC for Modular Multilevel Converter

In this subsection, conventional MPC is explained. For MMCs with conventional MPC, all the possible switching states are evaluated using a single cost function to obtain the optimal control of the output and circulating currents, and capacitors voltages [11]. The output and circulating currents equations for one step ahead is the same as (15) and (16). In this case, the voltage equation of the capacitor is rewritten as follows:

$$\frac{dv_{c,m,x}}{dt} = S\,\frac{i_{x,j}}{C_{SM}}, \tag{18}$$

where S indicates the switching state of each SM that if S = 1, the desired SM is in the circuit, and if S = 0, the SM is bypassed. Therefore, the equation of capacitor voltage with discretization by Euler first-order expansion are as follows:

$$V_c(k+1) = V_c(k) + S\,\frac{i_{x,j}}{C_{SM}}T_s, \tag{19}$$

By rewriting the cost function and adding the capacitor voltage term, the cost function is as follows [11]:

$$\begin{aligned} J = {} & \lambda_t \left| i_{t,j,\mathrm{ref}}(k+1) - i_{t,j}(k+1) \right| + \\ & \lambda_{cir} \left| i_{cir,ref}(k+1) - i_{cir,j}(k+1) \right| + \\ & \lambda_c \left(\sum_j \left| V_{c,j}(t+T_s) - \frac{V_{dc}}{N} \right| \right) \end{aligned} \tag{20}$$

In (20), all parameters are error absolute between the actual value and the reference value. The block diagram of the conventional MPC is shown in Fig. 5. According to this figure, the amount of the output and circulating currents and voltages of the capacitors are calculated for each switching state. Afterwards, by optimizing the cost function, the switching states are optimized and applied to MMC.

According to [11], in the conventional MPC and the overall valid switching states are considered, and the cost function is evaluated for each states. In conventional MPC, the volume calculations are significantly increased, hence to control a three-phase MMC with six SMs in each arm, the number of switching states is 924.

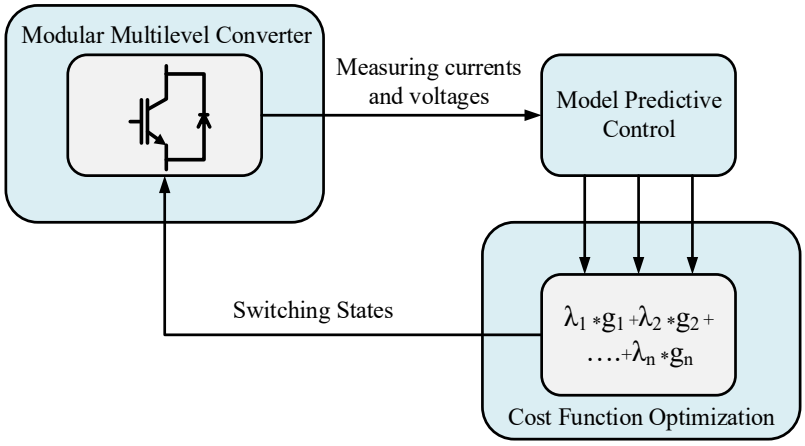

Fig. 5. Block diagram of the conventional MPC

Table 2. Comparison between the proposed method and three control methods in terms of the number of switching states: conventional MPC, indirect MPC, improved indirect MPC, and the proposed method.

Number of SMs (N)		4	10	50	100
Number of control states	FCS-MPC [11]	70	1.8×10^{5}	10^{29}	9.1×10^{58}
	Indirect FCS-MPC [12]	25	121	2601	10^{4}
	Improved indirect FCS-MPC [18]	5	11	51	101
	Proposed method	3	3	3	3

Comparison between the proposed method and different control methods in terms of the number of switching states are illustrated in Table 2. In all control methods, as the number of switching states increases, the computational volume and the complexity of the control system are increased, but by the proposed method, the switching states are significantly reduced, as shown in Table 2.

4- Simulation Results

In this section, a three-phase MMC is established in MATLAB/Simulink by the proposed method and conventional MPC to verify the proposed controller. The parameters are listed in Table 3. Some of the simulation parameters are determined based on the parameters [19], but the SM capacitor and arm inductance are calculated in next subsection. The active and reactive power references are set to 450kW and 120 kVar, respectively. The DC side voltage is 3.5kV, and voltage maximum of the AC side is 3.15kV. The number of SMs is 4 per arm. The capacitance in each SM is 10mF. The line inductance is 3.17mH, and the arm inductance is 5mH. In the simulations, three scenarios are considered as, scenario 1 steady-state operation, scenario 2 changing active and reactive power, and scenario 3 changing the output reference current. Fig. 6 shows the block diagram of the proposed system .

4- 1- . Selection of SM Capacitor and Arm Inductance

In this subsection, the parameters calculations of SM capacitor and arm inductance are explained.

The capacity of SM capacitor is obtained from the maximum energy stored in the capacitor and the apparent power of the converter. Therefore:

$$EP = \frac{E_{cmax}}{S_n} \tag{21}$$

where $E_{c,max}$, S_n and EP are the stored maximum energy in SM capacitor, apparent power, and energy-power rate of the converter, respectively. Typically, EP is between 10 J/kVA

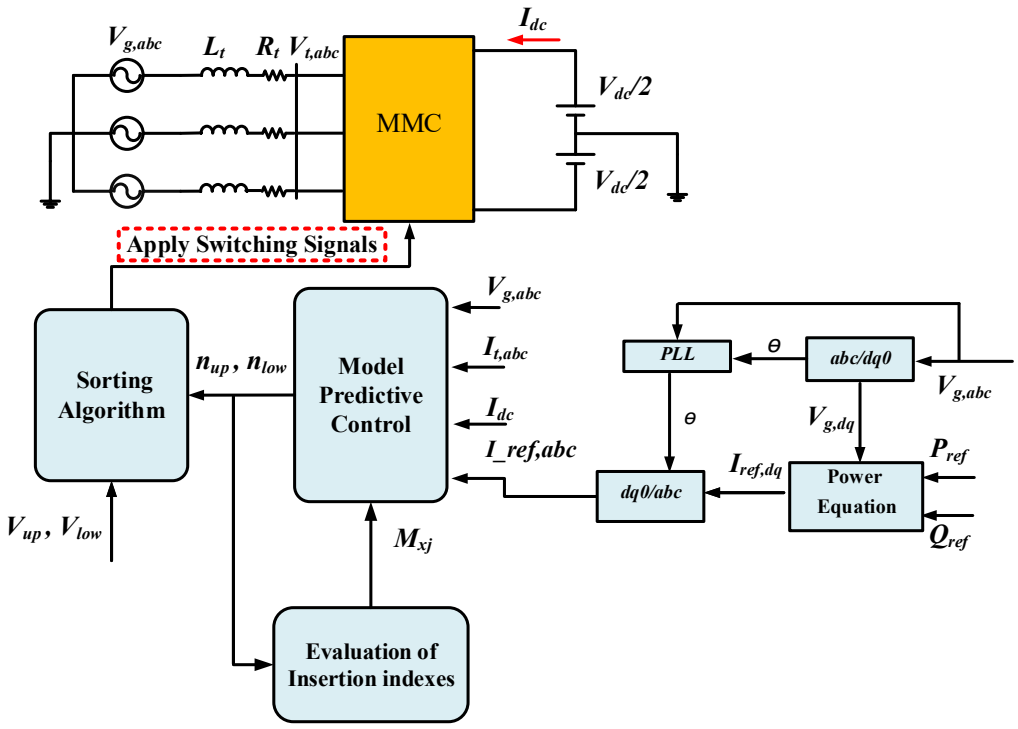

Fig. 6. The proposed control diagram

Table 3. Parameters of MMC

Parameters	Symbol	Simulation	Experimental
Nominal DC voltage	$V_{dc}/2$	3.5 (kV)	**60 (V)**
line to line AC voltage	$V_{t,j}$	3.15 (kV)	**60 (V)**
Active power	P	450 (kW)	**81.9 (W)**
Reactive power	Q	120 (kVar)	**27.75 (Var)**
Number of SMs	N	4	**6**
SM Capacitor voltage (V)	Vc	1750	**20**
SM capacitance (mF)	C	10	**2.2**
line resistance (Ω)	R_t	0.062	**-**
line inductance(mH)	L_t	3.17	**-**
resistance Arm (Ω)	R_{arm}	0.1	**0.2**
Arm inductance (mH)	L_{arm}	5	**4.07**
Sampling period (μs)	T_s	100	**200**
Output frequency (Hz)	f	50	**50**

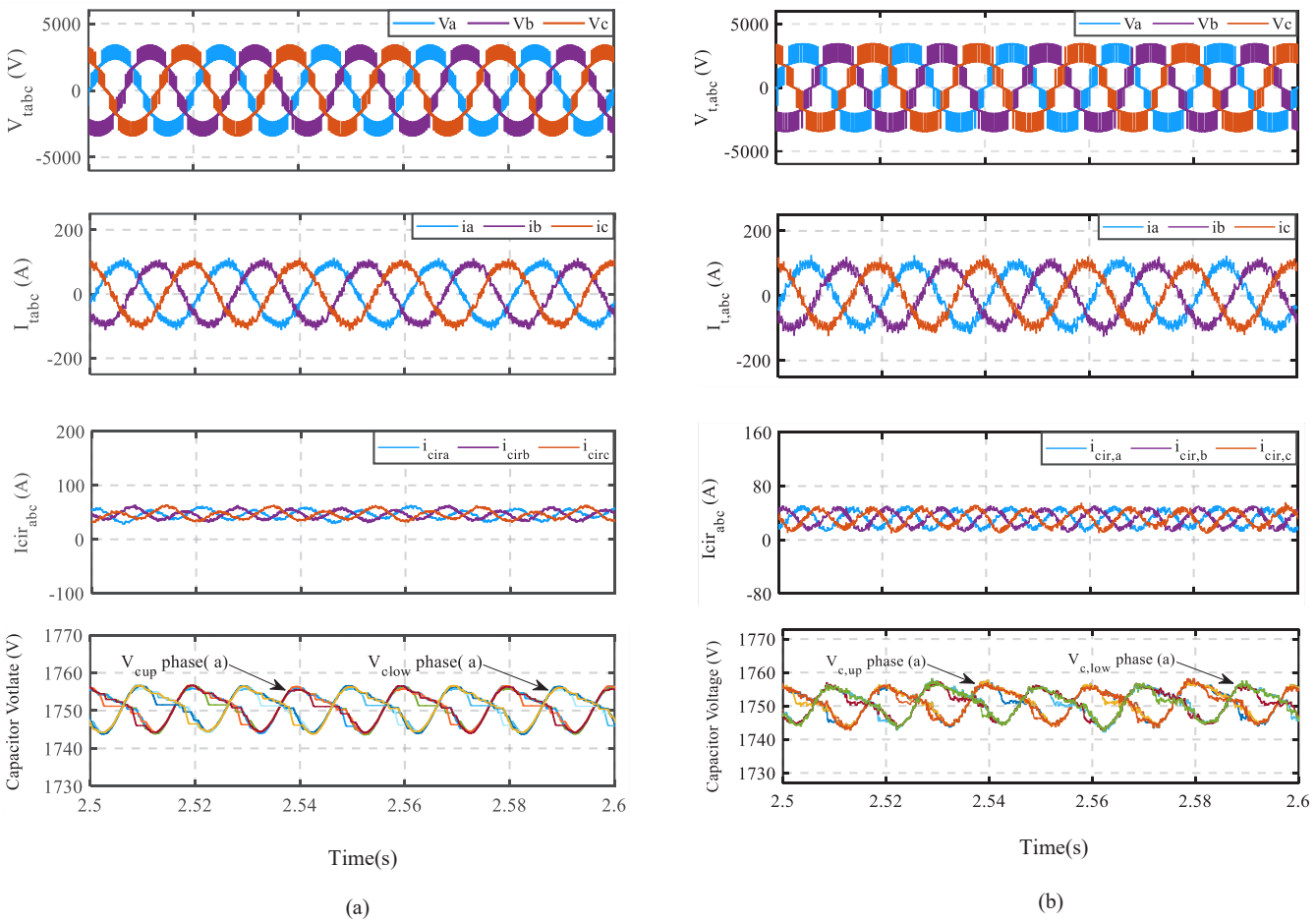

Fig. 7. Steady performance of MPC, (a) MMC is regulated by the proposed method (b) MMC with conventional MPC. From top to bottom, waveforms are output voltages, output currents, circulating currents and, SMs capacitors voltages.

and 50 J/kVA. When EP is decreased, the capacitor costs are reduced but the fluctuations of the capacitor voltage are increased. Hence, a tradeoff between the capacitor costs and the capacitor voltage fluctuations is needed.

The arm capacitance based on EP is calculated as follows [20]:

$$EP \frac{S_n}{3V_{dc}^2} \tag{22}$$

Then, the SM capacitance is as follow:

$$C = \frac{C_{arm}}{N} \tag{23}$$

where N is the number of SMs in each arm.

Therefore, the SMs capacitor is determined to equal 0.01 F.

The arm inductance is the main parameter to reduce the circulating current. Based on the resonant frequencies between the capacitors and the inductors, the appropriate constraint for determining the arms inductance size is obtained as follow:

$$L_s C > \frac{5N}{24\omega_1^2} \tag{24}$$

where ω_1 and L_s are the main frequency of the system, and the arm inductance in each phase (sum of the inductance of two arms). This equation determines the minimum inductance. Therefore, to prevent resonance in the converter arms, the arm inductance of each phase must be larger than the calculated value. Hence, the inductance for each arm is determined to equal 5 MH.

4- 2- Steady-state Operation

An MMC consisting of 4 SMs (N =4) is simulated in this subsection. The steady-state performance of the MMC regulated by the proposed method is illustrated in Fig. 7 (a). The output current and circulating current are well regulated with the proposed MPC, and the MMC operates stably with balanced SMs capacitors voltages. The voltage and current waveforms of the MMC with conventional MPC are shown in Fig. 7 (b) to compare.

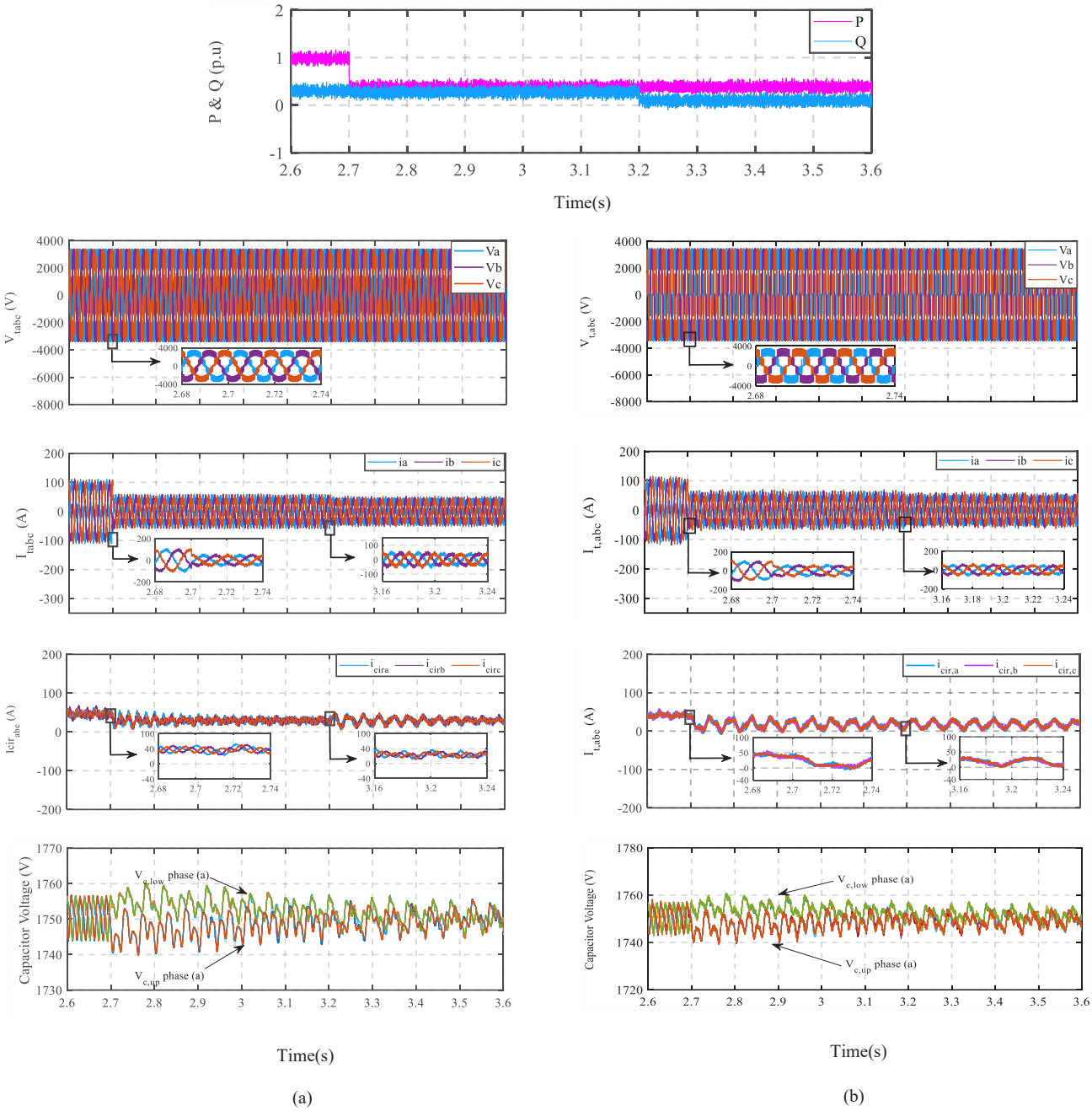

Fig. 8. Dynamic performance of MMC at the mode of changing active and reactive power, (a) MMC is regulated by the proposed method (b) MMC with conventional MPC. From top to bottom, waveforms are active and reactive power, output voltages, output currents, circulating currents and, SMs capacitors voltages.

According to Fig. 7, the proposed method presents fewer ripples in the output, circulating currents, and the output voltage. The converter generates five output voltage waveforms with 3.3 kV amplitude. The maximum amplitude of the output current is equal to 100 A by both control strategies, but the output current THD is 5.2% by the proposed method, while in the conventional MPC, the output current THD is 6.86%. Additionally, by applying the proposed method, the capacitors voltages fluctuations are lower than 1%. However, the fluctuations of the voltages of the capacitors are 1.57 %. Therefore, the proposed method gives better performance compared to the conventional MPC.

4- 3- Changing active and Reactive Power

To show the dynamic behaviors of the system, the active and reactive power are changed from 450 kW to 200kW at t=2.7s, and from 120 kVar to 50 kVar at t=3.2s, respectively as shown in Fig. 8. The dynamic operation of the system

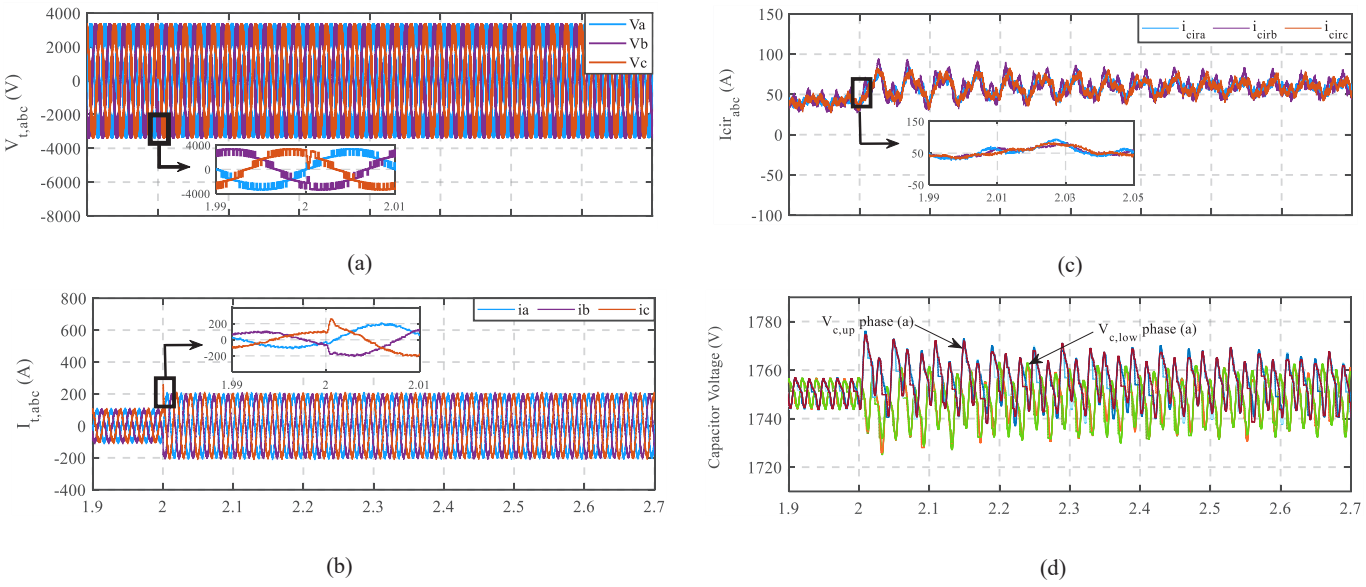

Fig. 9. Dynamic performance of MMC by the proposed method at the mode of changing the output current reference, (a) output voltages, (b) output currents, (c) circulating currents, (d) capacitors voltages.

regulated by the proposed method is illustrated in Fig. 8(a). Comparison with the conventional MPC, the voltage and current waveforms of the MMC are shown in Fig. 8(b).

According to Fig. 8(a), the three-phase output voltages remain constant at 3.3 kV before and after the change of active and reactive power. When the active power is changed, the output current quickly adapts to its reference. Additionally, by reducing the reactive power at t=3.2s to 50 kVar, the output current amplitudes by two control methods decrease, but the output current THD and oscillations by the proposed method are lower than compared to conventional MPC. In Fig. 8, the circulating currents are also shown, where they fluctuate around the DC value with limited amplitude before the power change. After reducing the active and reactive power, the DC component of the circulating current is reduced, but the system response with the proposed control method reaches the steady state faster compared to the conventional MPC. In addition, by applying the proposed method after the step changes, the voltage fluctuations of the capacitors are balanced around their nominal value, as shown in Fig. 8(a). However, since the active and reactive power decrease, the fluctuations amplitude of capacitors voltages with the proposed method and conventional MPC reduce to 0.79% and 1.33 %, respectively, which shows the proposed method compared to the conventional MPC gives the better performance.

4- 4- Changing the Output Current Reference

In this subsection, the dynamic behavior of the converter with the output reference current changing is shown. Primarily, the system is in steady-state operation, then the output current reference increases from 100A to 200A at t=2s. As shown in Fig. 9(a), after changing the output current reference, the number of output voltage levels does not change since the MMC output is connected to the grid and its voltage is constant. As shown in this figure, there are a few notches at this moment of changing reference. In addition, Fig. 9(b) shows the dynamic behavior of the output current with the output reference current changing. After changing the current reference, the measured output current properly follows its reference.

Fig. 9 (c) illustrates the circulating current with changing the reference current, where the circulating current fluctuates around its reference value with limited amplitude. The SMs capacitors voltages continue to be balanced at their reference value, as shown in Fig. 9(d). The reason behind the increasing voltage oscillation is the increasing in the arms power.

As a result, Fig. 9 verifies the dynamic behavior of the proposed method.

5- Experimental Results

To validate the proposed method, a single-phase MMC is built and tested. The power rating of the scaled prototype model is 81 W, which is restricted by the rating of the power supply used in the laboratory. The number of cells per arm is six. IGBTs with custom-designed gate drives are used as power semiconductor switches in the MMC. The converter feeds an inductance-resistive load. To implement the control strategy, Texas Instruments Microcontroller (TMS320F2812) is used. The parameters of the experimental setup are listed in Table 3. Due to microcontroller hardware limitation, T_s in the experimental setup is set to $200\,\mu s$. Fig. 10 (a) and Fig. 10 (b) show the laboratory setup and its components. To verify the proposed method's performance, the practical results are presented in the steady-state operation.

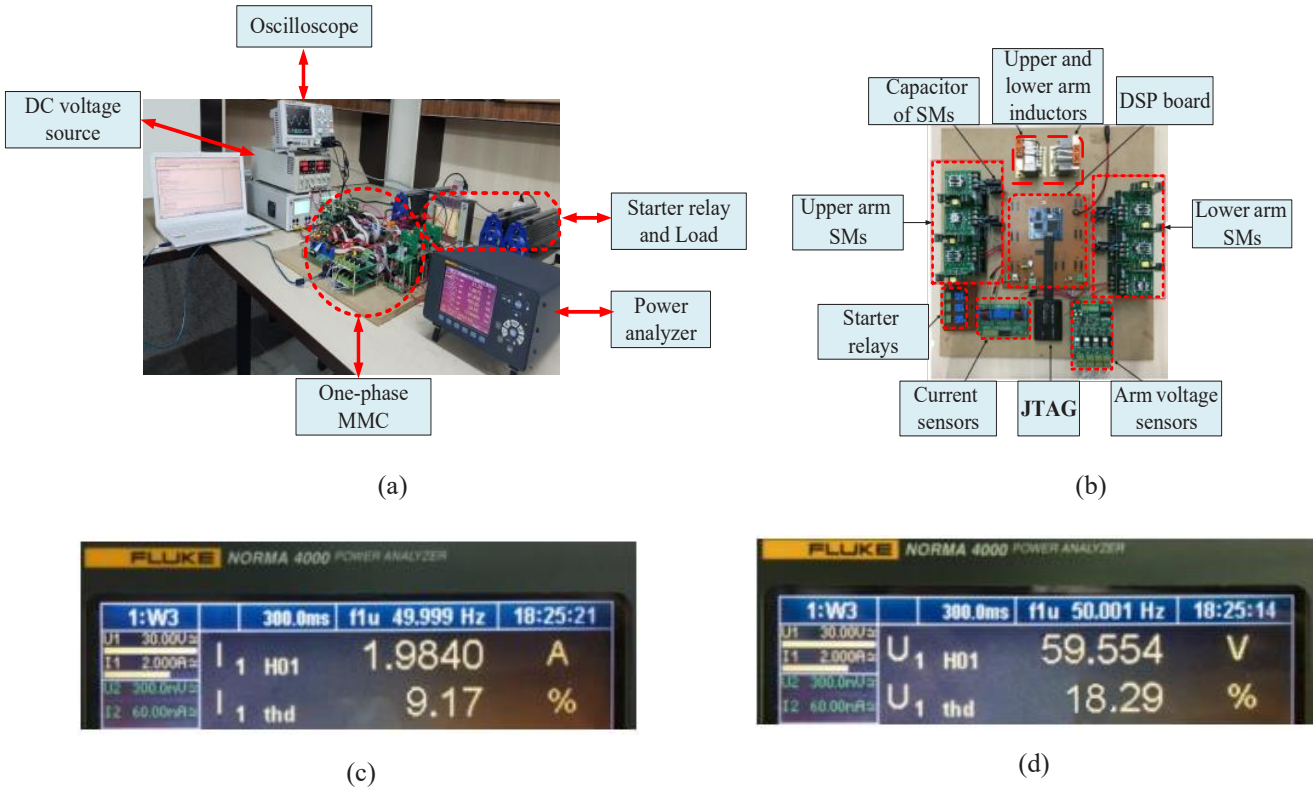

Fig. 10. Test bench setup and the scaled prototype model, (a) the prototype of 6 cells MMC, (b) control platform, (c) harmonic spectrums of the output current with the proposed method, (d) harmonic spectrums of the output voltage.

5- 1- Practical Results in Steady-state Operation

Fig. 11(a) shows the 7-level output voltage waveforms. The proposed method produces the desired output with an amplitude of half the DC voltage and frequency of 50 Hz periodically. Fig 11. (b) shows the laboratory result of the converter AC output current. The amplitude of the output current is 2A. Additionally, the dominant waveform of the output current is sinusoidal and has low harmonic components. To present the accuracy of the proposed method, the harmonic spectrums of the output current are shown in Fig. 10(c). In this figure, I_{thd} is calculated as:

$$I_{thd} = \frac{\sqrt{I_{rms}^2 - I_{h01}^2}}{I_{h01}}, \tag{25}$$

where, I_{ho1} and I_{rms} are the amplitude of the fundamental frequency component and RMS of the output current, respectively. As shown in Fig. 10(c), the output current THD of the MMC controlled by the proposed method is 9.17 %. Additionally, the output voltage THD is equal to 18.29% as illustrated in Fig. 10(d). Using the proposed method correctly, the upper arm capacitors voltages (V_{c1}, V_{c2}, and V_{c3}) follow the measured voltage at a nominal value of 20 V, as shown in Fig. 11(c). Finally, Fig. 11(d) shows the circulating current of the converter. One can observe that the current ripple resulting from the second-order harmonic that causes internal losses in the converter is effectively mitigated. The above-mentioned results verify the proposed method's performance in the steady state.

5- 2- Comparison of the Proposed Method and Indirect FCS-MPC in terms of Real-time Duration

With the proposed method, due to the calculation volume independence from the number of switching states, the real time duration (T_{DSP}) is significantly reduced. To calculate T_{DSP} by microcontrollers, several factors are affected such as the type of processor and its CPU, language, and method of coding, as well as code optimization. In the same conditions, the proposed methods and indirect FCS-MPC [12] are implemented on the MMC with four SMs in each arm by the Texas Instruments microcontroller (TMS320F2812), and T_{DSP} is measured for each method.

Due to microcontroller hardware limitations, the sampling period (T_s) is set to 200 μs. T_{DSP} of the proposed method and the indirect FCS-MPC are shown in Table 4. According to this table, the T_{DSP} of the proposed method and the indirect FCS-MPC are 35 μs. and 83 μs. respectively, which represent about 2.5 times faster for the proposed method. In addition, as the number of SMs increases in the indirect FCS-MPC, the computational burden and T_{DSP} increase; while in the proposed method, with reducing T_{DSP} the microcontroller speed increases.

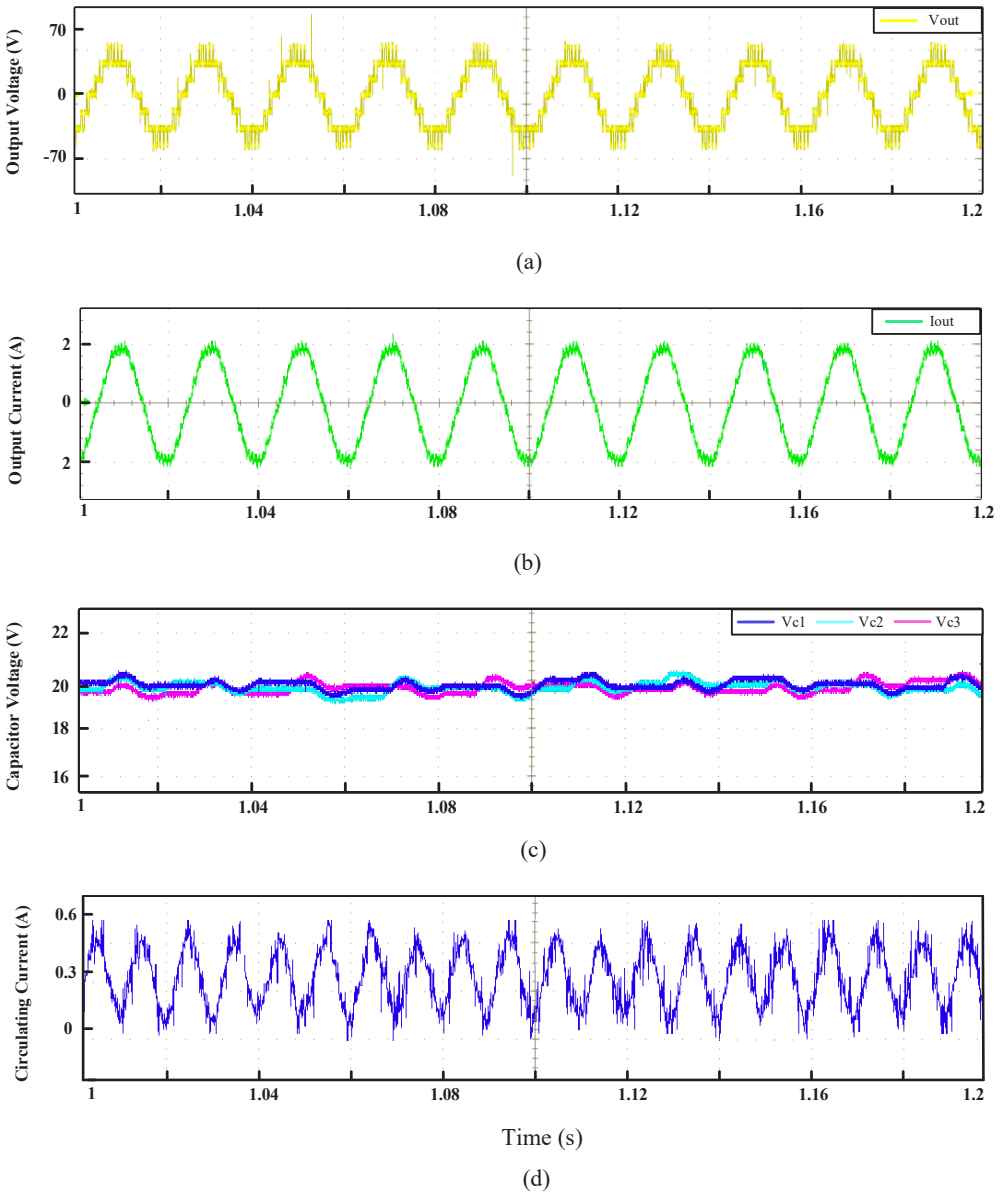

Fig. 11. Laboratory results of the steady state by the proposed method, (a) output voltage (b) output current (c) voltages of three upper arm capacitors (d) circulating current.

Table 4. Real-time duration comparison of the proposed method with indirect FCS-MPC

Table 4. Real-time duration comparison of the proposed method with indirect FCS-MPC

Control method / Real-time duration	Proposed method	Indirect FCS-MPC
T_{DSP}	35 μs	83 μs

6- Conclusion

In this paper, a simplified model predictive control is presented to reduce the computational burden of the predictive control for Modular Multilevel Converter compared to conventional MPC. In the proposed method, the optimal switching states can be achieved using the MMC state-space model and adjusting the switching states. Therefore, by a cost function, the most suitable number of inserted SMs for each arm suppresses the output current tracking error and the circulating current as well as retains the arms energy balancing. In addition, the proposed method improves the converter performance and reduces the settling time of the control system. The accuracy and precision of simplified model predictive control have been shown in different performance modes with simulation and experimental results.

List of Symbols

N	Number of sub-modules
j (a,b,c)	Phase of MMC
$L_{t,j}$	Line inductance, H
$R_{t,j}$	Line resistance, Ω
R_{arm}	Arm resistance, Ω
L_{arm}	Arm inductance, H
V_c	Capacitor voltage, V
$V_{cmi,j}$	Output voltage of the sub-module, V
C_{SM}	Sub-module capacitance, F
$i_{ci,j}$	Capacitor current, A
V_{dc}	Voltage on the DC side, V
$V_{up,j}$	Upper arm voltage, V
$V_{low,j}$	Lower arm voltage, V
$i_{up,j}$	Upper arm current, A
$i_{low,j}$	Lower arm current, A
$I_{t,j}$	Current of the grid, A
I_{dc}	DC side current, A
$V_{t,j}$	AC grid voltage, V
$i_{cir,j}$	Circulating current, A
x (upper/lower)	Arm of the converter
$i_{t,j}(k+1)$	AC grid predicted current, A
$i_{cir,j}(k+1)$	Predicted circulating current, A
T_s	Sampling time, s
J	Cost function
λ_{cir}	Weighting coefficient of the circulating current
λ_t	Weighting coefficient of the grid current
$M_{x,j}$	Taken feedback modulation index
n_{up}	Upper arm modulation index
n_{low}	Lower arm modulation index
$V_{x,j}$	Arm voltage, V
$V_{cmx,j}$	Voltage of each capacitor, V
$S_{mx,j}$	Switching signals
EP	Energy-power rate of the converter, J/kVA
$E_{c,max}$	Stored maximum energy, J
S_n	Apparent power, kVA
C_{arm}	Arm capacitance, F
ω_1	Main frequency of the system, Hz
L_s	Arm inductance in each phase, H
I_{thd}	output current THD
I_{h01}	Fundamental frequency component amplitude of output current, A
I_{rms}	RMS of the output current, A

f	grid frequency, Hz

References

[1] A. Pirhadi and M. T. Bina, "Design of DC-side fault current limiter for MMC-HVDC systems: Safety of the MMC along with frequency stability," vol. 14, pp. 2419–2429, 2020.

[2] Pan, Xicai, et al. "Circulating Current Analysis and Power Mismatch Elimination Strategy for an MMC-Based Photovoltaic System." 2020 IEEE Energy Conversion Congress and Exposition (ECCE). IEEE, 2020.

[3] Yu, Zixiang, et al. "Power Converter Topologies and Control Strategies for DC-Biased Vernier Reluctance Machines." IEEE Transactions on Industrial Electronics 67.6 (2019): 4350-4359.

[4] Harikumaran, Jayakrishnan, et al. "Failure modes and reliability-oriented system design for aerospace power electronic converters." IEEE Open Journal of the Industrial Electronics Society 2 (2020): 53-64.

[5] Kurochkin, Denis A., et al. "Multiport DC-DC Converter with Additional Inductance for Spacecraft Power Systems." 2020 21st International Conference of Young Specialists on Micro/Nanotechnologies and Electron Devices (EDM). IEEE, 2020.

[6] Deng, Fujin, et al. "Overview on submodule topologies, modeling, modulation, control schemes, fault diagnosis, and tolerant control strategies of modular multilevel converters." Chinese Journal of Electrical Engineering 6.1 (2020): 1-21.

[7] Bakbak, Ali, and Erkan Meşe. "An Approach for Space Vector PWM to Reduce Harmonics in Low Switching Frequency Applications." 2019 International Aegean Conference on Electrical Machines and Power Electronics (ACEMP) & 2019 International Conference on Optimization of Electrical and Electronic Equipment (OPTIM). IEEE, 2019.

[8] Mittal, Arvind, Kavali Janardhan, and Amit Ojha. "Multilevel inverter-based Grid Connected Solar Photovoltaic System with Power Flow Control." 2021 International Conference on Sustainable Energy and Future Electric Transportation (SEFET). IEEE, 2021.

[9] Hariri, Raghda, Fadia Sebaaly, and Hadi Y. Kanaan. "A Review on Modular Multilevel Converters in Electric Vehicles." IECON 2020 The 46th Annual Conference of the IEEE Industrial Electronics Society. IEEE, 2020.

[10] Song, Shuguang, and Jinjun Liu. "Interpreting the individual capacitor voltage regulation control of PSC-PWM MMC via consensus theory." IEEE Access 7 (2019): 66807-66820.

[11] J. Qin and M. Saeedifard, "Predictive control of a modular multilevel converter for a back-to-back HVDC system," IEEE Trans. Power Deliv., vol. 27, no. 3, pp. 1538–1547, 2012.

[12] M. H. Mohsen Vatani, Behrooz Bahrani, Maryam Saeedifard, "Indirect Finite Control Set Model Predictive Control of Modular Multilevel Converters," IEEE Trans. Smart Grid, vol. 6, no. 3, pp. 1520 – 1529, 2015.

[13] B. Gutierrez and S. S. Kwak, "Modular Multilevel Converters (MMCs) Controlled by Model Predictive Control with Reduced Calculation Burden," IEEE Trans. Power Electron., vol. 33, no. 11, pp. 9176–9187, 2018.

[14] Zhou, Dehong, Shunfeng Yang, and Yi Tang. "Model-predictive current control of modular multilevel converters with phase-shifted pulse width modulation." IEEE Transactions on Industrial Electronics 66.6 (2018): 4368-4378.

[15] M. Zhu and G. Li, "Modular Multilevel Converter with Improved Indirect Predictive Controller," IEEE J. Emerg. Sel. Top. Power Electron., vol. 7, no. 2, pp. 976–989, 2019.

[16] P. Münch, D. Görges, M. Izák, and S. Liu, "Integrated current control, energy control and energy balancing of modular multilevel converters," in Proc. 36th Annu. Conf. IEEE Ind. Electron. Soc. (IECON), Glendale, AZ, USA, 2010, pp. 150–155

[17] Karamanakos, Petros, and Tobias Geyer. "Guidelines for the design of finite control set model predictive controllers." IEEE Transactions on Power Electronics 35.7 (2019): 7434-7450.

[18] Wang, Yue, et al. "Model predictive control of modular multilevel converter with reduced computational load."2014 IEEE Applied Power Electronics Conference and Exposition-APEC 2014. IEEE, 2014.

[19] Q. Tu, Z. Xu, and L. Xu, "Reduced Switching-frequency modulation and circulating current suppression for modular multilevel converters," IEEE Trans. Power Deliv., vol. 26, no. 3, pp. 2009–2017, 2011.

[20] M. Zygmanowski, B. Grzesik, and R. Nalepa, "Capacitance and inductance selection of the modular multilevel converter," 2013 15th Eur. Conf. Power Electron. Appl. EPE 2013, 2013.

HOW TO CITE THIS ARTICLE

A. Sheybanifar, S. M. Barakati, Simplified Model Predictive for Controlling Circulating and Output Currents of a Modular Multilevel Converter. AUT J. Elec. Eng., 54(1) (2022) 121-136.

DOI: 10.22060/eej.2021.20393.5429